SCIENCE CHINA
Chemistry

• ARTICLES •
• SPECIAL TOPIC • Molecular Magnetism

June 2012 Vol.55 No.6: 967–972
doi: 10.1007/s11426-012-4570-5

Calixarene-supported hexadysprosium cluster showing single molecule magnet behavior

BI YanFeng[1], XU GuanCheng[2], LIAO WuPing[1*], DU ShangChao[1], DENG RuiPing[1] & WANG BingWu[2*]

[1]*State Key Laboratory of Rare Earth Resource Utilization; Engineering Research Center for the Separation and Purification of REs and Thorium, Changchun Institute of Applied Chemistry, Chinese Academy of Sciences, Changchun 130022, China*
[2]*Beijing National Laboratory for Molecular Sciences; State Key Laboratory of Rare Earth Materials Chemistry and Applications; College of Chemistry and Molecular Engineering, Peking University, Beijing 100871, China*

Received December 30, 2011; accepted January 13, 2012; published online April 10, 2012

The syntheses, crystal structures, magnetic and luminescent properties of three isomorphous compounds $[Ln^{III}_6(\mu_4\text{-}O)_2(C4A)_2(NO_3)_2(HCOO)_2(CH_3O)_2(DMF)_4(CH_3OH)_4]$ (Ln = Gd (**1**), Tb (**2**) and Dy (**3**); H_4C4A = *p-tert*-butylcalix[4]arene) are reported. These three compounds are featured with the sandwich-like units constructed by two tail-to-tail calixarene molecules and an in-between Ln^{III}_6 octahedron. The Dy^{III} compound exhibits both single molecule magnet behavior and photoluminescence.

calixarene, lanthanides, single molecule magnet, photoluminescence

1 Introduction

Lanthanides play a special role in the construction of molecular-based magnets due to their large angular momentum in the ground state and resulting huge Ising-type magnetic anisotropy in some cases [1, 2]. There have been many reports on the molecular magnets with lanthanides, especially dysprosium. However, the design and synthesis of such molecular magnets remain an exciting challenge owing to the fact that it is not easy to promote magnetic interactions between the 4f electrons of lanthanide ions through the bridging ligands [5, 6]. To deal with this problem, well-selected small and flexible ligands were chosen as the linkers to connect the paramagnetic metal centers [1–8]. An alternative approach is to entirely house the magnetic skeleton within a large and rigid "protective" organic or inorganic sheath, which has been proved to be a more effective method [9–11].

Calixarene and its derivatives, a class of macrocyclic polyphenol compounds, have shown good abilities in the construction of metal clusters owing to their inherent phenolic oxygen and easily modified functional groups [12–21]. The first poly-lanthanide compounds of calixarene were reported by Harrowfield and co-workers in the late 1980s [13], however, it is only in the last two years that several samples with single molecule magnet (SMM) behavior were reported by Dalgarno [14–16] and us [17]. Moreover, high-nuclearity (more than four metal centers) pure lanthanide-clusters supported by calixarenes were seldom concerned [18–22]. Here we present three hexalanthanide clusters sandwiched by two *p-tert*-butylcalix[4]arenes (H_4C4A, Scheme 1), $[Ln^{III}_6(\mu_4\text{-}O)_2(C4A)_2(NO_3)_2(HCOO)_2(CH_3O)_2(DMF)_4(CH_3OH)_4]$ (Ln = Gd (**1**), Tb (**2**) and Dy (**3**)) and their luminescent and magnetic properties. To the best of our knowledge, compound **3** presents the first example for the hexanuclear pure lanthanide cluster capped by calixarenes with single molecule magnet behavior.

*Corresponding authors (email: wpliao@ciac.jl.cn; bwwang@pku.edu.cn)

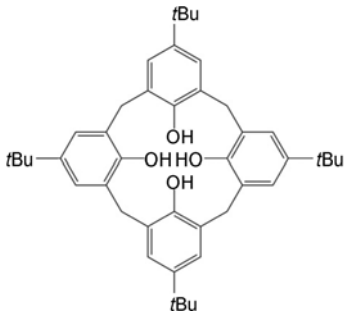

Scheme 1 Structure of *p-tert*-butylcalix[4]arenes (H_4C4A).

2 Experimental

2.1 General

p-tert-Butylcalix[4]arene (H_4C4A) was synthesized by literature method [23] and other reagents were purchased from commercial sources and used as received. FR spectra (KBr pellets) were taken on a Bruker Vertex 70 spectrometer. Powder X-ray diffraction (XRD) was determined by a Bruker D8 Advance diffractometer. Magnetic susceptibility measurements for **1–3** were performed on a Quantum Design MPMS XL-5 SQUID system. Diamagnetic corrections for the sample and sample holder were applied to the data.

2.2 Synthesis

Colorless single crystal blocks of **1–3** are obtained from reaction of the mixture of *p-tert*-butylcalix[4]arene (0.065 g, 0.1 mmol), $Ln(NO_3)_3{\cdot}6H_2O$ (0.068 g, ca.0.15 mmol, Ln = Gd (**1**), Tb (**2**), Dy (**3**)), $N(CH_2CH_3)_3$ (1 mL), DMF (5 mL), and CH_3OH (5 mL) in a 20 mL Teflon-lined autoclave which was kept at 130 °C for 3 days and then slowly cooled to 20 °C at about 4 °C/h. The crystals were isolated by filtration and then washed with 1:1 DMF-CH_3OH. Yield: ca. 30%, 45%, and 35% for **1–3** with respect to H_4C4A. The elemental analyses and FT-IR spectra (KBr pellets, cm^{-1}) of three compounds are similar and compound **1** was taken as an example: Element analysis (%), calcd: C 43.79, H 5.31, N 2.84; found: C 42.38, H 5.01, N 2.63; FT-IR: 3598(w), 3452(w), 3409(w), 2950(s), 2902(w), 2865(w), 2797(w), 1665(s), 1573(s), 1465(s), 1387(w), 1359(m), 1334(w), 1294(s), 1200(m), 1134(w), 1109(w), 1064(w), 1027(w), 960(w), 906(m), 866(m), 819(m), 803(m), 780(w), 738(m), 681(m), 542(w), 510(s), 482(m). Powder XRD measurements indicated the phase purity of the three compounds (Figure 1).

2.3 X-ray structure determination and refinement

The intensity data were recorded on a Bruker APEX-II CCD system with Mo-Kα radiation (λ = 0.71073 Å). The crystal structures were solved by means of Direct Methods and refined employing full-matrix least squares on F^2 (SHELXTL-97) [24]. All non-hydrogen atoms were refined anisotropically and hydrogen atoms of the organic ligands were generated theoretically onto the specific atoms and refined isotropically with fixed thermal factors. Hydrogen atoms on methanol molecules can't be generated and were included in the molecular formula directly. In addition, the high R_1 and wR_2 factor of compounds **1–3** might be due to the weak high-angle diffractions and the disorder of *tert*-butyl atoms. The crystal structures for complexes **1–3** have been deposited at the Cambridge Crystallographic Data Centre and allocated the deposition numbers CCDC 802372–802374. The crystal data and cell parameters for **1–3** are summarized in Table 1.

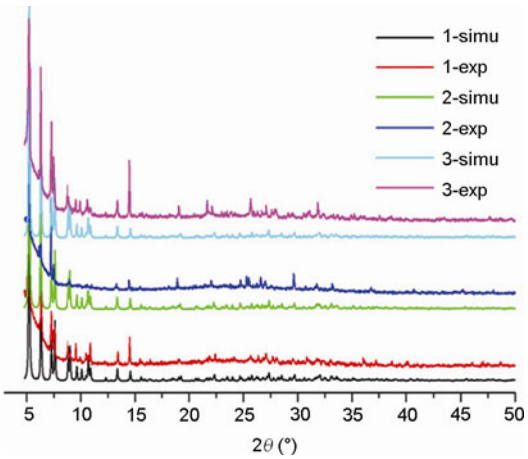

Figure 1 Simulated and experiment XPRD patterns of **1–3**.

Table 1 Data collection and refinement statistics of **1–3**

	1	**2**	**3**
Formula	$C_{108}H_{156}Gd_6N_6O_{30}$	$C_{108}H_{156}Tb_6N_6O_{30}$	$C_{108}H_{156}Dy_6N_6O_{30}$
Formula wt.	2961.89	2971.91	2993.39
Cryst. syst	triclinic	triclinic	triclinic
Space group	$P\bar{1}$	$P\bar{1}$	$P\bar{1}$
a (Å)	11.8444(4)	11.8493(3)	11.8708(4)
b (Å)	14.5554(5)	14.5023(4)	14.5126(5)
c (Å)	17.3045(6)	17.3226(5)	17.3109(6)
α (°)	101.6900(10)	101.8210(10)	101.8940(10)
β (°)	93.7770(10)	93.7760(10)	93.7430(10)
γ (°)	98.8360(10)	98.9830(10)	98.9210(10)
V (Å^3)	2872.20(17)	2863.01(14)	2863.01(14)
Z	1	1	1
D_c (g cm^{-3})	1.712	1.720	1.736
μ (mm^{-1})	3.490	3.724	3.941
F (000)	1470	1476	1482
Tot. data	17629	17423	24406
Uniq. data	10164	10019	10135
R_{int}	0.0180	0.0212	0.0163
GOF	1.082	1.105	1.126
$R1$[a] $[I > 2\sigma(I)]$	0.0289	0.0344	0.0252
$wR2$[b](all data)	0.0854	0.1005	0.0801

a) $R1 = \Sigma||F_0|-|F_c||/\Sigma|F_0|$; b) $wR2 = \{\Sigma[w(F_0^2-F_c^2)^2]/\Sigma[w(F_0^2)^2]\}^{1/2}$.

3 Results and discussion

3.1 Crystal structures

Single-crystal X-ray diffraction determinations reveal that the features of **1**–**3** are given by the sandwich-like units composed by an in-between Ln^{III}_6 core and two tail-to-tail calixarene molecules (Figure 2). Isomorphous compounds **1**–**3** crystallize in a triclinic system with space group $P\bar{1}$. On the basis of the structure determination and charge-balance considerations, these three structures can be formulated as $[Ln^{III}_6(\mu_4\text{-O})_2(C4A)_2(NO_3)_2(HCOO)_2(CH_3O)_2(DMF)_4(CH_3OH)_4]$. The formate anions found in the structures can be assigned to the decomposition of DMF. There are three crystallographic sites for the metal ions (Ln1, Ln2, and Ln3). Seven-coordinated Ln1 site is bonded by four phenoxo oxygen atoms from one C4A with a cone conformation, two μ_4-O, and one methanol oxygen. Both Ln2 and Ln3 are coordinated by two phenoxo oxygen atoms from two different C4As, one μ_4-O, one methanol μ_2-O atom, and one formate oxygen atom. Two left coordination sites of seven-coordinated Ln2 are occupied by two oxgen atoms from DMFs while three rest coordination sites of eight-coordinated Ln3 are occupied by two nitrate oxygen atoms and one methanol oxygen atom. It should be noted that the methanol molecule in μ_2-O mode is deprotonated and the Ln2/Ln3-μ_2-O distances (being of 2.315(3)/2.296(3) Å) are much shorter than those with unprotonated methanols (Ln1-O13, 2.546(3)Å; Ln3-O12, 2.472(4) Å, taking **3** as an example, hereafter the same). Such assignment is consistent with charge-balance considerations and also found for the $V^{III}V_5^{IV}$-C4A compound [22].

Ln1, Ln2, Ln3 and three metal sites generated by the symmetry operations are bridged by eight phenoxo oxygen atoms, two μ_4-O, and two μ_2-O of methanol molecules to form a Ln_6 clusters with an octahedral arrangement of the metals (Figure 2). The octahedron edge distances (Ln···Ln) are in the range of 3.5780(3)–3.6193(2) Å. The Ln–O–Ln angles are in the range of 100.72(10)–112.39(12)°, which are larger than those in the planar Dy^{III}_4 core bonded by thiacalix[4]arene [17]. It is noted that Ln2–Ln3–Ln2* and Ln3–Ln2*–Ln3* angles are of 90.56° and 89.44°, that is, the Ln2, Ln3, Ln2* and Ln3* are obviously coplanar. The sandwich-like units of **1**–**3** can also be described by the capping of two Ln–C4A units on a planar Ln_4 core. These two tail-to-tail calixarenes adopting the cone conformation are parallel to each other and located on a same axis as those in a Ln_4-thiacalix[4]arene cluster [17] but different from those in the $Mn^{II}_2Mn^{III}_2$–$(C4A)_2$ SMM [14]. The Ln_6 cluster is perfectly encapsulated and protected by the organic shell. Furthermore, the sandwich-like Ln_6-$(C4A)_2$ units are well separated to each other with the shortest distance between two paralleled units being of 11.85 Å (center to center, Figure 3) and the shortest intermolecular Dy···Dy separation distance is of 8.26 Å. No obvious intermolecular interaction was observed between two adjacent Ln_6-$(C4A)_2$ units except weak hydrogen bonds between DMF ligand and NO_3^- (C(51)–H(51b)···O(8), 3.172(9)Å, 120°).

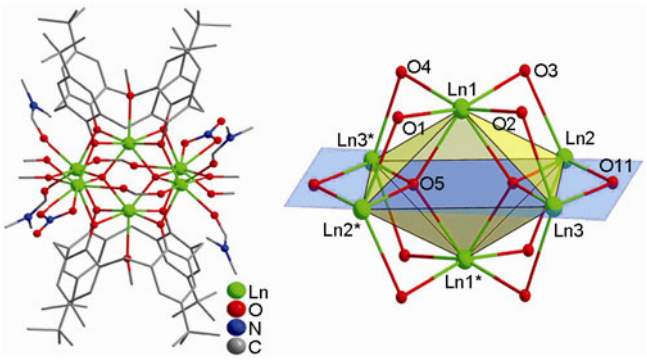

Figure 2 Molecular structures of compounds **1**–**3** (left) and the magnetic cores showing the arrangement of six Ln^{III} ions (right). The hydrogen atoms are omitted for clarity.

3.2 Magnetic properties of 1–3

Both dc and ac magnetic susceptibilities of **1**–**3** were measured with the freshly prepared polycrystalline samples. The dc magnetic susceptibilities of **1**–**3** were measured in an applied magnetic field of 1 kOe between 300 and 2 K (Figures 4 and 5). At 300 K, the $\chi_M T$ values of 47.12, 71.03, and

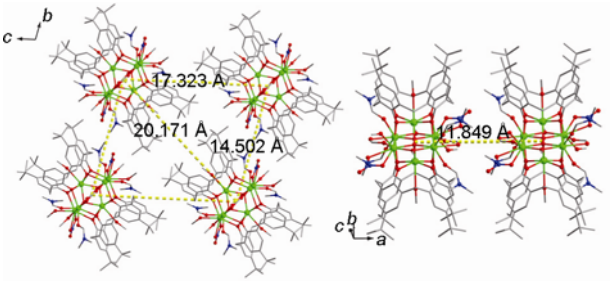

Figure 3 Extended structures of **1**–**3** showing the distances between two sandwich units

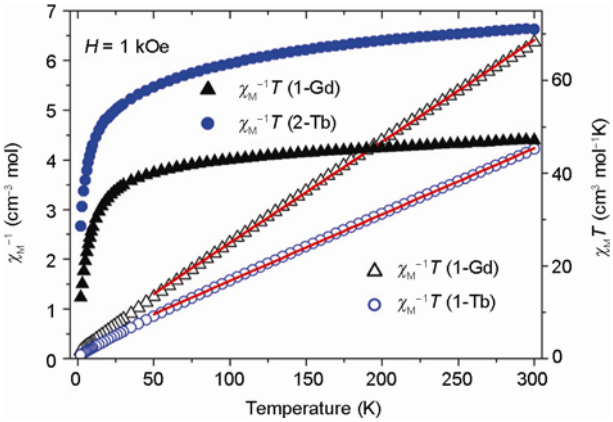

Figure 4 Plots of $\chi_M T$ vs. T and $1/\chi_M$ vs. T for **1** and **2** in a 1 kOe field. Red lines represent the Curie-Weiss fitting.

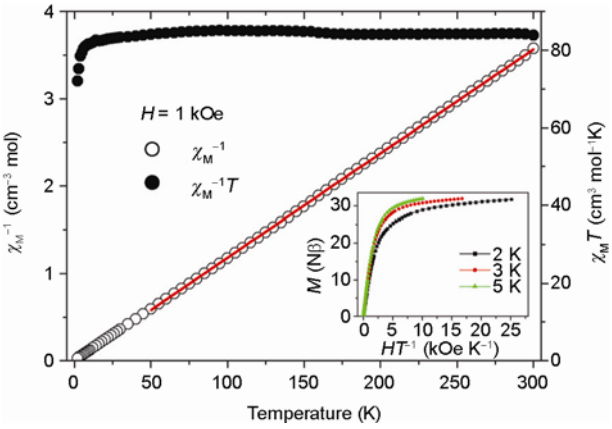

Figure 5 Plots of $\chi_M T$ vs. T and $1/\chi_M$ vs. T for **3** in a 1kOe field. Red line represents the Curie-Weiss fitting. Insert: M-HT^{-1} plot of **3** at 2, 3 and 5 K.

83.82 cm^3 K mol^{-1} for **1**–**3** are close to the expected values of 47.28, 70.92, and 85.02 cm^3 K mol^{-1} for six uncoupled Ln^{III} ions, respectively. Upon cooling, the $\chi_M T$ values gradually decrease and reach the minimum values of 13.22 and 28.56 cm^3 K mol^{-1} at 2 K for **1** and **2**, respectively. As the spin-orbit coupling of Gd^{3+} ion is very small, the decrease of the $\chi_M T$ values indicates that the exchange coulping interactions between Gd^{3+} ions are antiferromagnetic. Whereas the $\chi_M T$ value of **3** remains roughly constant with decreasing temperature down to 14 K, and then drops rapidly to a minimum value of 72.04 cm^3 K mol^{-1} at 2 K. Owing to the orbital contribution and ligand field effect, there is no appropriate theoretical model to describe the change of magnetic susceptibility quantitatively for Dy^{3+} clusters. If assuming the contribution of the exchange part is similar with the Gd^{3+} system of **1**, the much slower decrease of the $\chi_M T$ values with lowering temperature indicated that the ground and low-lying excited states of compound **3** may possess the component of large total angular momentum, which is very important for displaying magnet-like behavior.

Furthermore, the field dependence of the magnetization of **3** at different temperatures shows a rapid increase in the magnetization at low field, which eventually reaches 31.74 Nβ at 2 K under 50 kOe dc field. This value is lower than the expected saturation value of 60 Nβ (for six Dy^{III} ions) but close to that of other reported Dy^{III} compounds (6×5.23 Nβ) [1–6], which can be also ascribed to the anisotropy of Dy^{III} ion and crystal-field effects. The non-superposition of the temperature-dependence at different fields (Figure 5 insert) implies the presence of a significant magnetic anisotropy in compound **3** [1–6].

Fitting the experimental data ranging from 50 to 300 K to Curie-Weiss law gives Curie constants (C) of 49.33, 75.10, and 83.53 cm^3 mol^{-1} K and Weiss constants (θ) of –14.11, –17.19, and 1.06 K for **1**–**3**, respectively. The small negative Weiss constant (θ) for **1** containing spin-only Gd^{3+} ions suggests dominant antiferromagnetic interactions between spin carriers. For the Tb^{3+} ion is magneitc anisotropic center, the Stark sub-levels depopulation is also possibly responsible for the negative Weiss constant of **2**. Moreover, no peaks were observed in the out-of-phase of ac susceptibility (χ'') for **1** and **2** (Figure 6). All these results indicate there is no single-molecule-magnet behavior for **1** and **2** above 2 K.

Given the resemblance of the $\chi_M T$ vs. T and M vs. H plots to the Dy^{III}_4 SMM with a large anisotropic barrier [5], the dynamics of the magnetization of **3** was investigated from the ac susceptibility measurements. The ac susceptibilities of **3** show obvious frequency-dependent both in- (χ') and out-of-phase (χ'') under a zero dc field ranging from 0.4 to 15 K (Figure 7). The frequency-dependence of χ'' peaks at about 2 K is indicative of SMM behavior. Additionally, according to the frequency dependence of in-phase (χ') susceptibilities, we get $\phi = (\Delta T_p/T_p)/\Delta(\log f) = 0.28$ (T_p: the temperature of the maximum; f: the frequency of the oscillating field), which is in the range of superparamagnet, and excluded the possibility of the spin glass state. However, another Dy^{III}_6 cluster with similar coordination was reported to show no signs of slow magnetic relaxation [21]. The energy barrier of thermal-assisted slow magnetization relaxation and characteristic relaxation time can be obtained by fitting the peak temperatures with Arrhenius law (Figure 8), giving $U_{eff} = 7.6$ K and $\tau_0 = 1.1 \times 10^{-6}$ s. There are anothor frequency-dependent χ'' peaks at about 6 K, which are obvious at 1500 Hz and 1000 Hz, but unconspicuous at lower frequency. These peaks indicate that there is a second mag-

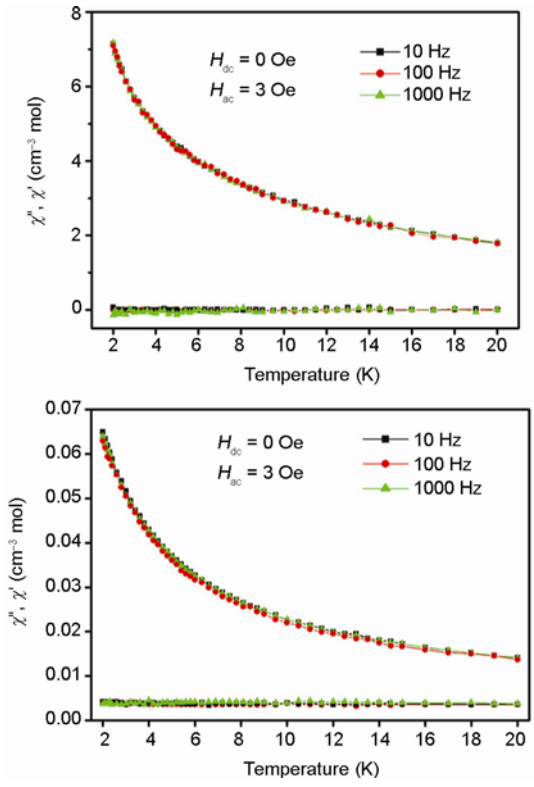

Figure 6 ac susceptibility measurements for **1** (upper) and **2** (bottom).

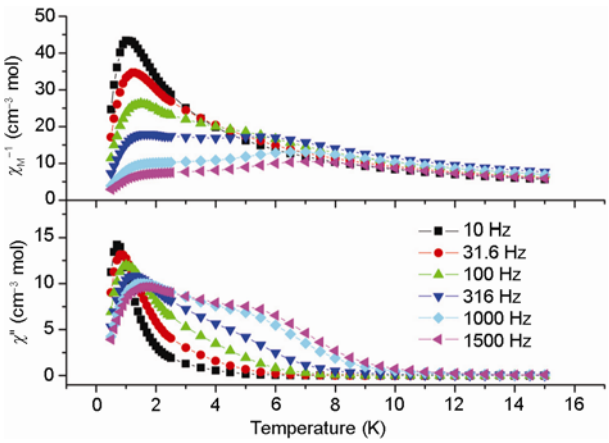

Figure 7 Temperature dependence of the in-phase (top) and out-of-phase (bottom) components of the ac magnetic susceptibility for **3** in a zero dc field.

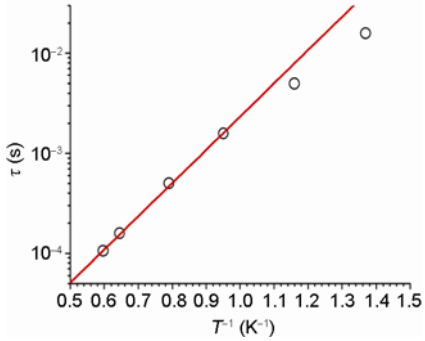

Figure 8 Arrhenius plot for compound **3**.

netic relaxation process at about 6 K. Those two points deviated to the linear region of Arrhenius plot are also the results of second relaxation. By the limitation of our SQUID magnetometer, the energy barrier of the second relaxation hasn't been obtained. Taking into account the geometry structures of compound **3**, the multi-relaxation may come from different sites of Dy^{III} ions. Although the estimation of the characteristic parameters (U_{eff} and τ_0) of Dy^{III}_6-$(C4A)_2$ compound might not be very accurate, the first single molecule magnet of pure lanthanide clusters of H_4C4A can be nominated as U_{eff} and τ_0 have magnitudes similar to those of other SMM systems.

3.3 Photoluminescent properties of 1–3

As continuous investigation of luminescent and magnetic bifunctional materials of calix[4]arene [17], the solid-state luminescence of compounds **1–3** was investigated at room temperature (Figure 9). Upon excitation at 329 nm, compound **2** shows a green luminescence and the obtained emission spectra can be ascribed to the characteristic f→f transitions (626, 586, 545 and 492 nm, $^5D_4 \rightarrow {}^7F_J$ (J = 3, 4, 5, 6)) of Tb^{III}. There are three main peaks at 395, 421, and 470

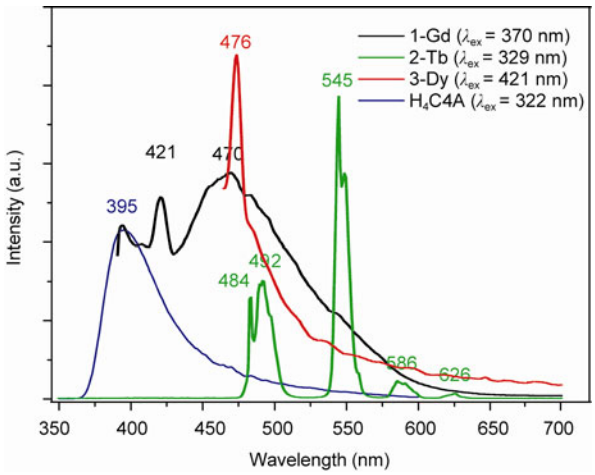

Figure 9 Luminescent spectra of **1**–**3** and H_4TC4A in the solid state at room temperature.

nm in the emission spectra of **1** (λ_{ex} = 370), which can be assigned to the ligand fluorescence because H_4C4A exhibits broad emissions in the region of 350–600 nm with a peak at 395 nm. Only one emission peak at 476 nm was found for **3**, which can be assigned to the $^4F_{9/2} \rightarrow {}^6H_{15/2}$ transitions of Dy^{III}. The fact that ligand-based luminescence was observed for **1** and **3** while not for **2**, indicates that the H_4C4A ligand transfers energy more efficiently to Tb^{III} than to Gd^{III} or Dy^{III}.

4 Conclusions

We prsented a hexadysprosium cluster sandwiched between two tail-to-tail calixarenes and its two analogous. The Dy_6 cluster gives another example for the pure lanthanide clusters isolated by calixarenes and showing SMM behavior. Due to the photoluminescent properties of calixarene and lanthanides, this work would also shed light on the design and synthesis of novel molecule-based multifunctional materials.

This work was financially supported by the National Natural Science Foundation of China (20971119, 51074148, 91026024). The authors wish to thank Prof. Song Gao for the magnetic measurement and helpful discussion on magnetism.

1 Tang JK, Hewitt I, Madhu NT, Chastanet G, Wernsdorfer W, Anson CE, Benelli C, Sessoli R, Powell AK. Dysprosium triangles showing single-molecule magnet behavior of thermally excited spin states. *Angew Chem Int Ed,* 2006, 45: 1729–1733
2 Chibotaru LF, Ungur L, Soncini A. The origin of nonmagnetic kramers doublets in the ground state of dysprosium triangles: Evidence for a toroidal magnetic moment. *Angew Chem Int Ed,* 2008, 47: 4126–4129
3 Hussain B, Savard D, Burchell TJ, Wernsdorfer W, Murugesu M. Linking high anisotropy Dy3 triangles to create a Dy6 single-molecule magnet. *Chem Commun,* 2009, 1100–1102

4 Lin PH, Burchell TJ, Clérac R, Murugesu M. Dinuclear dysprosium(III) single-molecule magnets with a large anisotropic barrier. *Angew Chem Int Ed,* 2008, 47: 8848–8851

5 Lin PH, Burchell TJ, Ungur L, Chibotaru LF, Wernsdorfer W, Murugesu M. A polynuclear lanthanide single-molecule magnet with a record anisotropic barrier. *Angew Chem Int Ed,* 2009, 48: 9489–9492

6 Guo YN, Xu GF, Gamez P, Zhao L, Lin SY, Deng RP, Tang JK, Zhang HJ. Two-step relaxation in a linear tetranuclear dysprosium (III) aggregate showing single-molecule magnet behavior. *J Am Chem Soc,* 2010, 132: 8538–8539

7 Xu GF, Wang QL, Gamez P, Ma Y, Clérac R, Tang JK, Yan SP, Cheng P, Liao DZ. A promising new route towards single-molecule magnets based on the oxalate ligand. *Chem Commun*, 2010, 46: 1506–1508

8 Aromí G, Brechin EK. *Struct Bonding*. Berlin: Springer, 2006, 122: 1–69

9 Ishikawa N, Sugita M, Ishikawa T, Koshihara S, Kaizu Y. Lanthanide double-secker complexes functioning as magnets at the single-molecular level. *J Am Chem Soc,* 2003, 125: 8694–8695

10 Ishikawa N, Sugita M, Wernsdorfer W. Nuclear spin driven quantum tunneling of magnetization in a new lanthanide single-molecule magnet: bis(phthalocyaninato) holmium anion. *J Am Chem Soc,* 2005, 127: 3650–3651

11 AlDamen MA, Clemente-Juan JM, Coronado E, Martí-Gastaldo C, Gaita-Ariño A. Mononuclear lanthanide single-molecule magnets based on polyoxometalates. *J Am Chem Soc,* 2008, 130: 8874–8875

12 Kajiwara T, Iki N, Yamashita M. Transition metal and lanthanide cluster complexes constructed with thiacalix[*n*]arene and its derivatives. *Coord Chem Rev,* 2007, 251: 1734–1746 and references therein

13 Harrowfield JM, Ogden MI, White AH, Wilner FR. Lanthanide ion complexes of the calixarenes. part 4. Double inclusion by *p-t*-butylcalix[4]arene (H_4L). crystal structures of $[Eu_2(HL)_2(dmf)_4]\cdot 7dmf$ (dmf = dimethylformamide) and $H_4L\cdot$dmso (dmso = dimethyl sulphoxide). *Aust J Chem,* 1989, 42: 949–958

14 Karotsis G, Teat SJ, Wernsdorfer W, Piligkos S, Dalgarno SJ, Brechin EK. Calix[4]arene-based single-molecule magnets. *Angew Chem Int Ed*, 2009, 48: 8285-8288

15 Karotsis G, Kennedy S, Teat SJ, Beavers CM, Fowler DA, JMorales J, Evangelisti M, Dalgarno SJ, Brechin EK. $[Mn^{III}_4Ln^{III}_4]$ calix[4]arene clusters as enhanced magnetic coolers and molecular magnets. *J Am Chem Soc,* 2010, 132: 12983–12990

16 Taylor SM, McIntosh RD, Beavers CM, Teat SJ, Piligkos S, Dalgarno SJ, Brechin EK. Calix[4]arene supported clusters: a dimer of $[Mn^{III}Mn^{II}]$ dimmers. *Chem Commun*, 2011, 47: 1440-1442

17 Bi YF, Wang XT, Liao WP, Wang XW, Deng RP, Zhang HJ, Gao S. Thiacalix[4]arene-supported planar Ln_4 (Ln = Tb^{III}, Dy^{III}) clusters: Toward luminescent and magnetic bifunctional materials. *Inorg Chem,* 2009, 48: 11743–11747

18 Fleming S, Gutsche CD, Harrowfield JM, Ogden MI, Skelton BW, Stewart DF, White AH. Calixarenes as aryloxides: Oligonuclear europium(III) derivatives. *Dalton Trans,* 2003, 3319–3327

19 Kajiwara T, Wu HS, Ito T, Iki N, Miyano S. Octalanthanide wheels supported by *p-tert*-butylsulfonylcalix[4]arene. *Angew Chem Int Ed,* 2004, 43: 1832–1835

20 Kajiwara T, Katagiri K, Takaishi S, Yamashita M, Iki N. A dodecalanthanide wheel supported by *p-tert*-butylsulfonylcalix[4]arene. *Chem Asian J,* 2006, 1: 349–351

21 Sanz S, McIntosh RD, Beavers CM, Teat SJ, Evangelisti M, Brechin EK, Dalgarno SJ. Calix[4]arene-supported rare earth octahedral. *Chem Commun*, 2012, 48: 1449–1451

22 Aronica C, Chastanet G, Zueva E, Borshch SA, Clemente-Juan JM, Luneau D. A mixed-valence polyoxovanadate(III,IV) cluster with a calixarene cap exhibiting ferromagnetic V(III) –V(IV) Interactions. *J Am Chem Soc*, 2008, 130: 2365–2371

23 Gutsche CD, Iqbal M, Stewart D. Calixarenes. 19. Syntheses procedures for p-tert-butylcalix[4]arene. *J Org Chem,* 1986, 51: 742–745

24 Sheldrick GM. A short history of SHELX. *Acta Crystallogr Sect A*: *Fundam Crystallogr*, 2008, 64: 112–122